JOURNAL OF GEOPHYSICAL RESEARCH, VOL. 86, NO. A6, PAGES 4511–4516, JUNE 1, 1981

Whistler Mode Wave Propagation in the Solar Wind Near the Bow Shock

E. W. GREENSTADT,[1] R. W. FREDRICKS,[1] C. T. RUSSELL,[2]
F. L. SCARF,[1] R. R. ANDERSON,[3] AND D. A. GURNETT[3]

The presence of whistler mode waves in, and upstream from, the bow shock has been well established by observation. Theoretical descriptions of the mode under solar wind conditions have been relatively meagre, however, and it may not be generally appreciated how readily whistler waves generated in the shock could occupy most of the region ahead of the shock most of the time. Graphic descriptions of phase and group velocities and group velocity directions for typical solar wind parameters are presented by using the cold plasma approximation over all appropriate frequencies and directions with respect to the IMF. The relations of whistler phase and group velocities to observations of a quasi-perpendicular shock crossing by ISEE are illustrated.

INTRODUCTION

The 'whistler' wave mode solution of the plasma dispersion relations for small amplitude waves [*Stix*, 1962] is invoked to explain many phenomena in the earth's plasma environment. In a recent capsule review, *Al'pert* [1980] describes four decades of whistler studies, referencing about 200 papers or, by his estimate, perhaps 10% of the total literature on whistlers. The great bulk of whistler observations has been in the magnetosphere, and numerous mathematical properties of the wave mode have been explored and exploited in applying the theory to the observations. We may even include the Jovian magnetosphere in this generalization [*Menietti and Gurnett*, 1980; *Coroniti et al.*, 1980]. Outside the magnetosphere in the solar wind, however, comparable investigation is still relatively primitive. In particular, the earth's bow shock is an established site for whistlers, both as standing waves [*Perez and Northrop*, 1970; *Guha et al.*, 1972; *Greenstadt et al.*, 1975; *Fairfield and Feldman*, 1975] and as propagating waves [*Smith et al.*, 1967; *Heppner et al.*, 1967; *Olson et al.*, 1969; *Fairfield*, 1974; *Rodriguez and Gurnett*, 1975, 1976], but only relatively easy connections of measurement to phase velocities have been examined. Contemporary experimental capabilities now encourage study of this mode at high resolution with full attention to spectral, directional, phase, and group velocity details. We expect these details to become increasingly important in understanding the full complement of phenomena in the foreshock outside the quasi-parallel portion of the bow shock [*Greenstadt and Fredricks*, 1979], where whistlers of some frequencies can easily propagate upstream at fairly large angles to the interplanetary magnetic field (the IMF). In this report we offer some views of the whistler mode that include its group velocity properties, albeit still in an abridged, cold plasma approximation.

We present some three-dimensional plots of phase and group velocity for representative solar wind conditions, confining ourselves here to frequencies above the ion-cyclotron frequency f_{ci} (for protons). We then display the magnetic observations at a quasi-perpendicular shock crossing by ISEE 1 and 2 and the corresponding whistler group velocity plots. Finally, we discuss the relationship of the observations to the depicted wave properties.

EQUATIONS

We use a simple, cold plasma wave formula, the Appleton-Hartree approximation, valid when $f \gg f_{ci}$. From *Stix* [1962, p. 40], we obtain phase velocity

$$U_\phi^2 = c^2 \left(\frac{f_{ce}}{f_{pe}}\right)^2 \left[\frac{f}{f_{ce}} \cos\theta - \left(\frac{f}{f_{ce}}\right)^2\right] \tag{1}$$

where $c = 3 \times 10^5$ km/s, f_{ce}, f_{pe} are electron cyclotron and plasma frequencies, and θ is the angle between the IMF $\mathbf{B}$ and $\mathbf{k}$. The group velocity is then given by

$$\mathbf{u}_g = \frac{d\omega}{d\mathbf{k}} = \frac{\partial\omega}{\partial k}\hat{\mathbf{k}} + \frac{1}{k}\frac{\partial\omega}{\partial\theta}\hat{\boldsymbol{\theta}}$$

where $\hat{\mathbf{k}}$ and $\hat{\boldsymbol{\theta}}$ are perpendicular unit vectors. The magnitude of the group velocity is then found from

$$U_g^2 = \frac{U_\phi^2}{\cos^2\theta}\,[4(\cos\theta - f/f_{ce})^2 + \sin^2\theta] \tag{2}$$

and its direction in terms of angle θ_g between $\mathbf{B}$ and $\mathbf{U}_g$ from

$$\tan\theta_g = \sin\theta\,\frac{\cos\theta - 2f/f_{ce}}{\cos\theta(\cos\theta - 2f/f_{ce}) + 1} \tag{3}$$

The key approximations made in deriving expression (1), hence (2) and (3) as well, are $f_{pe}^2 \gg f_{ce}^2$ and $f^2 f_{ce}^2 \sin^4\theta \ll 4\cos^2\theta$. Both are easily satisfied for most θ in the solar wind plasma of interest here. Since the approximations inherent in deriving the above expressions introduce increasing error as θ approaches 90°, we have cut off all calculations at $\theta = 80°$.

For this report, we picked one set of solar wind parameters representing the 'most probable' solar wind, combining values from the peaks of the parameter distributions [*Diodato et al.*, 1974; *Formisano et al.*, 1974], plus some fast and slow stream cases representing the range of likely conditions.

PHASE AND GROUP VELOCITY SURFACES

Figure 1 shows two plots of U_ϕ versus f/f_{ce}, the dashed one representing the cold plasma Appleton-Hartree (A-H) approximation, and the other representing the more general expression of *Formisano and Kennel* [1969, equation 2.7]. The positions of the ion-cyclotron (*ci*) and lower hybrid (*LH*) frequencies are indicated on the abscissa. Above $f/f_{ce} = 0.01$, the

[1] Space Sciences Department, TRW Defense and Space Systems Group, Redondo Beach, California 90278.
[2] Institute of Geophysics and Planetary Physics, University of California, Los Angeles, California 90024.
[3] Department of Physics and Astronomy, University of Iowa, Iowa City, Iowa 52242.

Paper number 80A1521.
0148-0227/81/080A1521

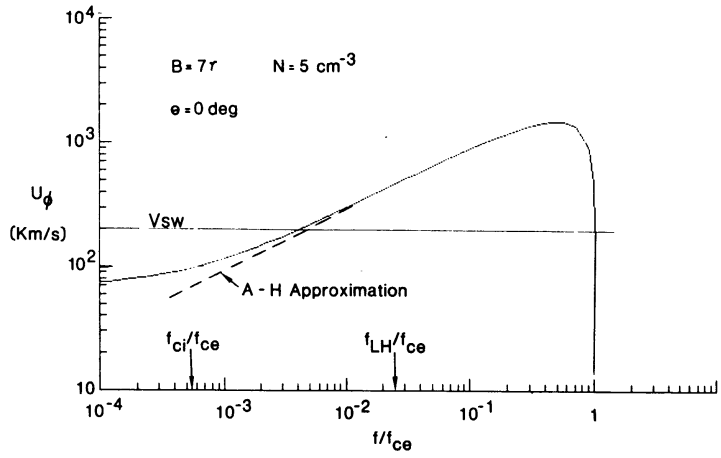

Fig. 1. Comparison of cold plasma, phase velocity dispersion curve with more general solution above f_{ci} at $\theta = 0$.

A-H approximation is a quite acceptable version of whistler behavior, and above f_{LH}, where the remainder of this report concentrates, the two curves are virtually identical.

The average solar wind parameters applicable to these curves are printed at the upper left in the figure. Note that the example is for propagation at a single angle, $\theta = 0$, and that a true depiction of whistler properties must include all angles.

The general behavior of whistler phase propagation in the solar wind setting is illustrated in Figure 2, following one branch of (1), for a range of realistic solar wind parameters. In each computer sketch, U_ϕ is plotted vertically against θ_ϕ and f/f_{ce}, all on linear scales. The axes are labelled in the largest sketch at the right. Phase angle θ is subscripted with symbol ϕ for phase to emphasize its distinction from group velocity direction θ_g discussed later. The horizontal curves in the U_ϕ surfaces above the θ-f plane represent the appropriate solar wind speed V_{sw} in each graph. All shaded portions of the U_ϕ surfaces above V_{sw} correspond to whistler waves whose phase velocities exceed V_{sw} and whose phase fronts can therefore propagate directly against the solar wind away from the bow shock at its subsolar point. The maximal U_ϕ in each surface occurs at $f = 0.5 f_{ce}$, $\theta_\phi = 0$. The plots at left represent three 'typical' conditions, and the fourth, at right, a less common one, that accompanied a laminar bow shock reported in detail a few years ago. The parameter combinations at left, top to bottom, represent average, faster than average, and slower than average solar wind, with the field and density values chosen according to their statistical correlations. The combination at right prevails occasionally when low Mach number bow shock crossings are observed [*Greenstadt et al.*, 1975; *Fairfield and Feldman*, 1975]. The figure shows that wave energy in the whistler mode can appear to advance against the solar wind in almost every probable solar wind condition for most frequencies below f_{ce}, and even for an improbable, low Mach number case. Since low Mach number means the bow shock appears much further away than usual, the extremely high U_ϕ's at such times imply, further, that the presence of the earth's shock may be detectable at great distances from the earth. Analogous reasoning applied to the Jovian shock suggests that it should not be surprising to encounter signals from Jupiter occasionally at great distances from that planet.

A major distinction between phase and group velocities arises from the difference in direction between the two vectors; that is, the angle θ_g of the group velocity with respect to the field differs from θ_ϕ. This difference can be appreciated by viewing the graph of (3) in Figure 3, where θ_g is plotted vertically against θ_ϕ and f/f_{ce}. We see that the angle θ_g never exceeds about 20°, at $\theta_\phi \approx 55°$ and zero frequency. For all f/f_{ce}, θ_g has a maximum at $\theta_\phi \lesssim 55°$, and θ_g is actually negative for all θ_ϕ when $f > 1/2\ f_{ce}$. The net result is a distorted and double-valued group velocity surface when represented in the format of Figure 2, as follows.

The group velocity surface of one branch of (2), corresponding to the average conditions of the upper left case in Figure 2, is shown in the lower graph in Figure 4. The corresponding graph of U_ϕ is repeated above the U_g plot for comparison on the same scale. Each curve making up the U_g surface corresponds to a constant θ_ϕ curve in the U_ϕ surface; the skewing caused by the disparity between θ_ϕ and θ_g, described by Figure 3, is evident in the twist of the constant θ_ϕ curves composing the U_g surface. Note that for positive θ_g ($f < 0.5 f_{ce}$), the U_g surface is double valued; as θ_ϕ increases, U_g decreases until $\theta_g \lesssim 20°$, then folds back on itself. The small inserts in Figure 4 separate the two overlapping parts of the U_g surface for $\theta_\phi < 55°$ and $\theta_\phi > 55°$. It is clear that group velocities exceed phase velocities over most of the frequency range so that not only phase fronts, but wave energy as well, can propagate against the solar wind for almost all angles and all frequencies at which the velocities are defined.

APPLICATION

The application of the foregoing calculations is illustrated in the case of a quasi-perpendicular bow shock crossing by ISEE 1 on November 7, 1977. The shock was timed from ISEE 1 to ISEE 2 and found to be expanding at 5.5 km/s. The two central panels of Figure 5 show the profiles of the IMF magnitude and ecliptic Z component for the crossing at 2251:20 UT. The depicted shock profile is reasonably 'typical' of the bow shock at high Alfvén Mach number ($M_A \gtrsim 5$), high beta ($\beta \approx 1$), and quasi-perpendicular angles ($70° \lesssim \theta_{Bn} \lesssim 90°$; n refers to the shock normal), when moving slowly (<10 km/s) and observed at high resolution ($\gtrsim$ one sample per second). The 'foot' preceding the shock from 2251:00 to 2251:20 is related to the region of residence of ions reflected by, and trapped in, the shock and clearly contains waves of many frequencies from 0 to f_{ce}. The exact structure of the foot has yet to be determined with all diagnostics. The stacked panels above B_Z display 11 channels of the University of Iowa/TRW

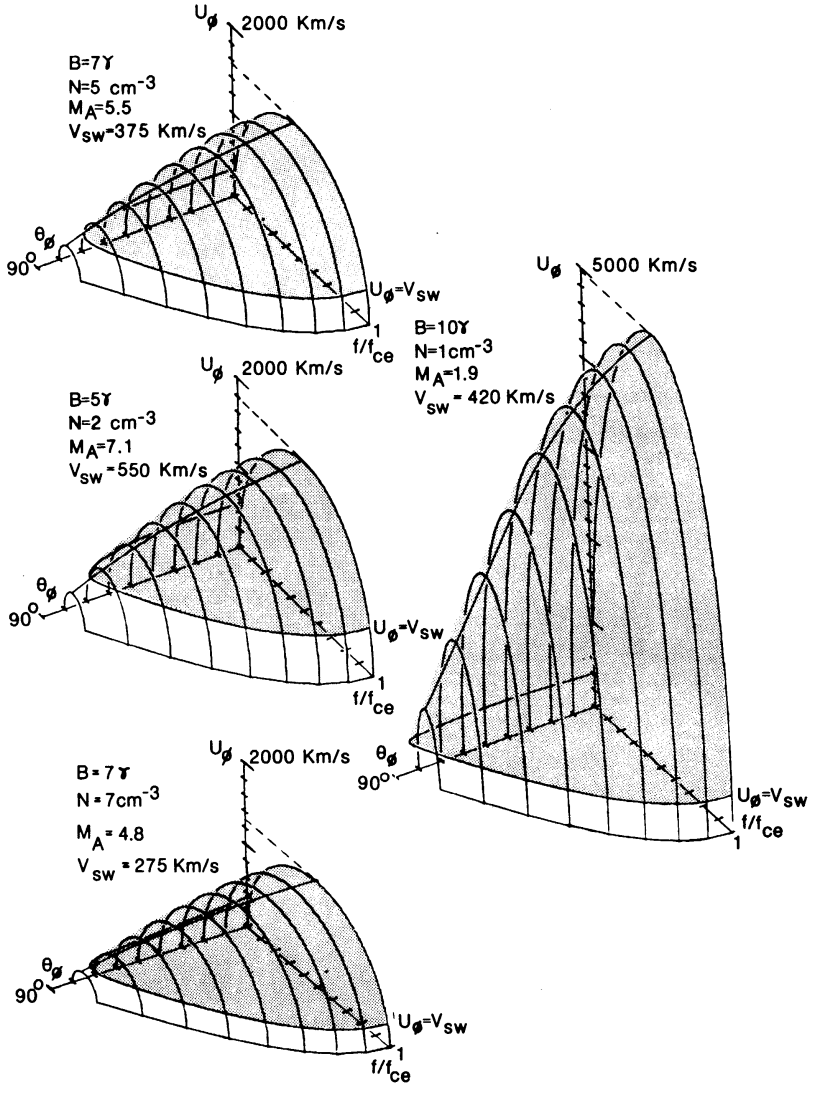

Fig. 2. Three-dimensional plots of phase velocity U_ϕ versus angle θ_ϕ of **k** to **B** and frequency f/f_{ce}, in the solar wind under four representative conditions. Upper left: most probable solar wind. Middle left: fast stream. Lower left: slow stream. Right: low Mach number. Shading designates velocity above solar wind speed.

magnetic wave analyzer [*Gurnett et al.*, 1978]. Wave noise appeared above background in the 17.8 and 31.1-Hz channels at 2250:27, immediately following the shift in IMF direction visible in B_Z. The noise subsided at 2250:35 in conjunction with a second directional change in B_Y (not shown) and reappeared again at 2250:50 at the outermost toe of the foot of the bow shock. The dotted curve crossing several of the channels calls attention to the staggered onset of noise at different frequencies. The string of large dots indicates roughly the relative position among the channels of the electron cyclotron frequency f_{ce}.

When the 31 and 17.8-Hz noise first initiated the foot of the shock, the upper and lower wave frequency cutoffs were $\approx 0.22f_{ce}$ and $0.12f_{ce}$, f_{ce} being 140 Hz in the solar wind. In the three-dimensional plot of whistler U_g at bottom left of the figure, the dashed line from the f/f_{ce} axis leads to the portion of the U_g surface cutoff at about 31 Hz. Allowing for some uncertainty in the actual cutoff frequency, the shaded strip of the U_g surface above V_{sw} indicates the ranges of θ, θ_g, and U_g applicable at the leading edge of the foot. The implied propagation geometry is shown in the sketch immediately above where the corresponding lightly shaded sectors define phase propagation U_ϕ at almost every angle to **B** and energy propagation U_g essentially along plus or minus **B** or the shock surface (within ±20°), the two being effectively indistinguishable within the propagation cone in this case. Dark shading indicates θ_ϕ, θ_g overlap.

At 2251:15, deep in the foot of the shock, the IMF rose to an average of about 10 γ, making $f_{ce} \cong 280$ Hz. The wave noise at that time occupied every channel up to f_{ce} and above, the bursts in higher channels attributable to peaks in the variable B where $f_{ce} > 280$ Hz. The plot of U_g at bottom right indicates by shading that the waves could have been whistlers propagating in a wide cone with respect to $-\mathbf{B}$ at any $f/f_{ce} < 1$. Note that since only one of the two symmetric wave solutions is illustrated, there is actually a similar wide cone of group propagation with respect to $+\mathbf{B}$; i.e., the true wave picture is symmetric parallel and antiparallel to **B**.

The lines crossing at the circle representing the satellite position in the shock sketch above the U_g surface at bottom left are meant to signify that whistlers reaching ISEE 1 (symmetrically) at that time would have come from locations on the

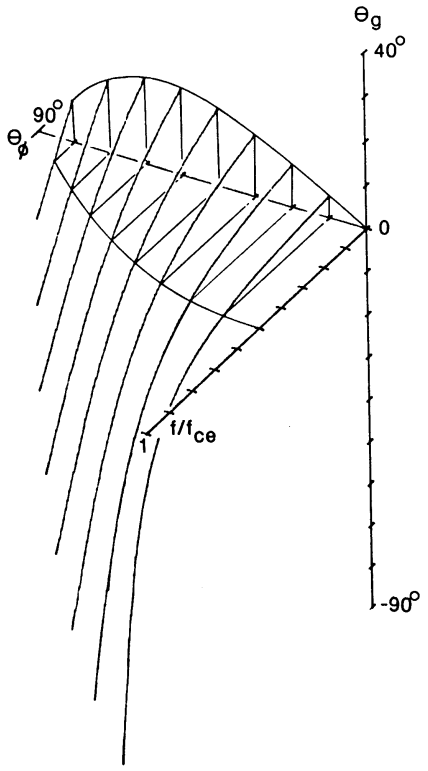

Fig. 3. Group velocity direction θ_g, with respect to the IMF, versus phase velocity direction θ_ϕ and f/f_{ce} for most probable solar wind.

shock laterally removed from the spacecraft position. Just before crossing, in the corresponding sketch at right, the wider propagation cone and close proximity of shock to spacecraft imply that observed waves originated on the shock much closer to the actual crossing point.

DISCUSSION

Whistler propagation in the solar wind, even at frequencies and angles where the simplest cold plasma approximation is permissible, has moderately complicated properties not well represented by assuming $f \approx 0$ or $\theta_g \approx \theta_\phi$. One way of matching analysis of this mode to observation, less awkward and more effective visually than X-Y plotting of families of curves for many angles, is to produce computer drawn three-dimensional sketches such as those shown in this report. When applied to magnetic field observations of the foot of a quasi-perpendicular bow shock recorded at frequencies from zero to well above f_{ce}, the sketches contribute to the interpretation of the whistler structure of the foot.

The observations tell us that the foot had a 'layered' wave composition: Waves of 15 to 30 Hz reached furthest upstream from the (magnetic) shock surface. As distance to the shock decreased, waves of both lower and higher frequencies were added to the wave environment with noise in most bands increasing in amplitude as the shock was approached. The classical foot, visible in the dc profile made by the UCLA magnetometer, appeared at 2251. The stable nature of the layered wave structure was evidenced when a 'notch' in the conventional foot appeared, marked by the pair of close, parallel vertical dashed lines at about 2251:05 in the enclosed panels of Figure 5. During that brief episode, which we assume was occasioned by a temporary, small retreat of the shock in the course of its more persistent expansion, the wave noise dropped significantly at and above 56 Hz, but not at lower frequencies, implying that the satellite was returned temporarily to the layer it had passed through at about 2250:59.

If we remember that the shock was travelling outward at an average speed of about 5.5 km/s, then its distance from ISEE 1 when the 31-Hz waves first appeared 30 s before the crossing was about 165 km. The analytic sketches tell us that these forwardmost waves could not have been propagating more than about 10° to the shock surface and could not have reached the spacecraft from a position on the shock closer than about 900 km away from the local crossing point. Propagating at smaller angles to **B**, they could have come from an area of the shock several thousand km away laterally. The higher frequency, 'inner' waves seen later, 3 s from the crossing, on the other hand, could have reached the spacecraft at angles up to about 55° from **B** and no further than a few km from the local crossing point. Moreover, the same waves, even though propagating more slowly under the less favorable plasma conditions earlier at 2250:50, could easily have reached the satellite then, but obviously were not observed. Similarly, there is no characteristic of the group velocity surfaces that would explain why 31-Hz waves were not recorded further upstream than they were; i.e., earlier than 2250:50. We know from the data of Figure 5 that the full spectrum of waves up to f_{ce} was generated in

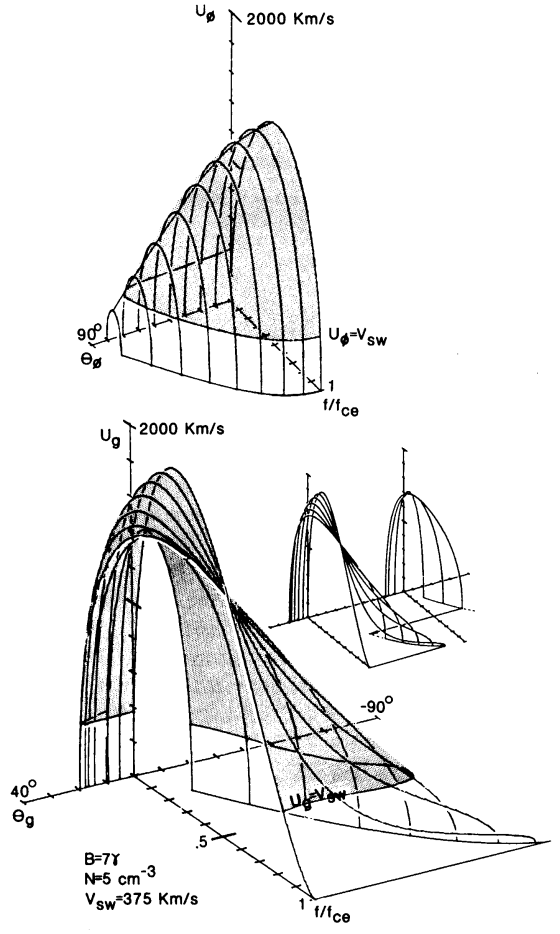

Fig. 4. Phase and group velocity plots versus corresponding directions θ_ϕ, θ_g, and f/f_{ce} for most probable solar wind. Curves of constant θ_ϕ form the surfaces in both cases; shading as in Figure 2. Inserts at right separate the sheets forming the double-valued U_g surface.

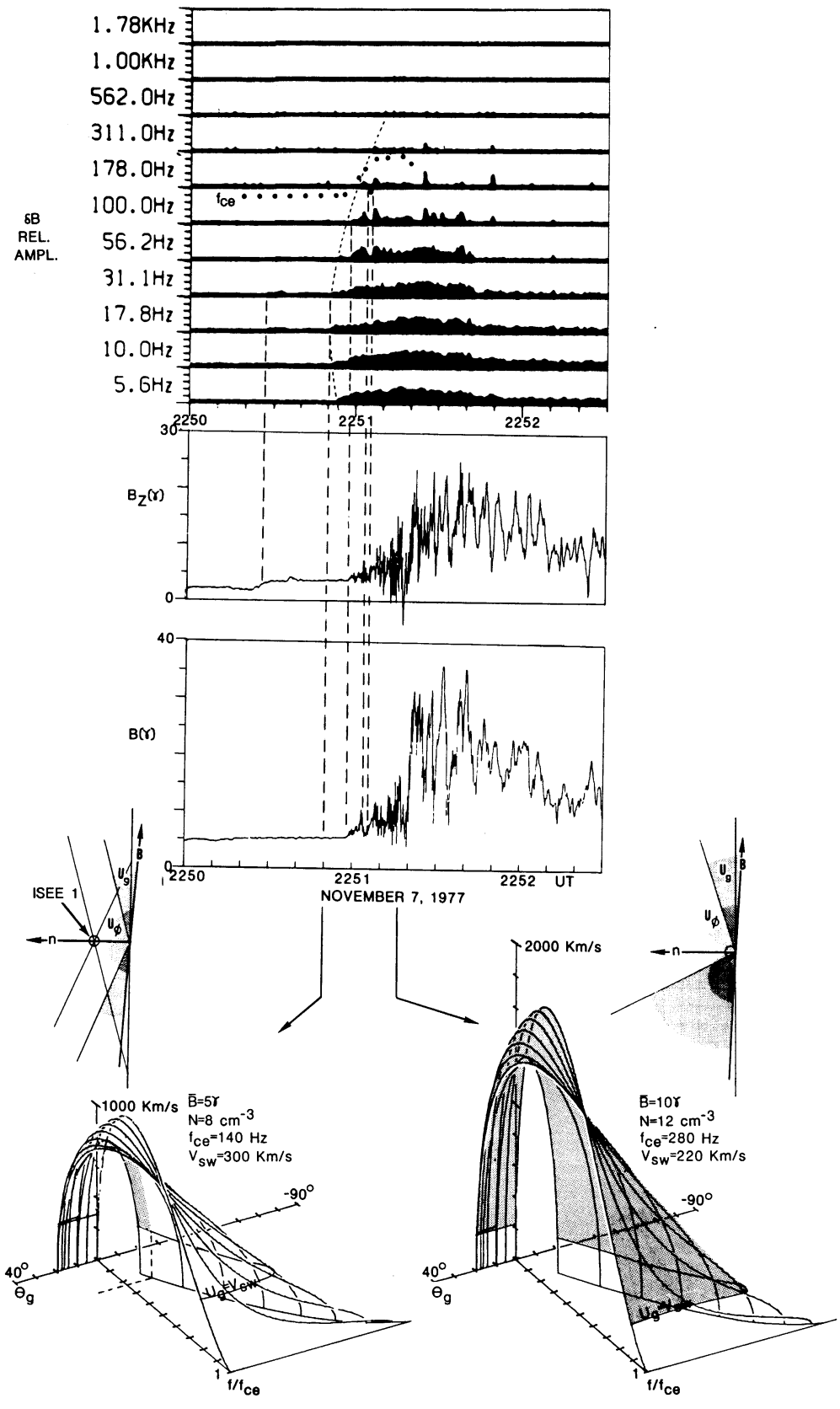

Fig. 5. Shock crossing by ISEE 1 showing staggered foot in magnetic noise channels and two related group velocity surfaces.

the shock; the sketches and the staggered activation of the various channels demonstrate that spectrally and/or directionally determined damping of whistlers was taking place in the leading edge of the shock foot. Several other cases for which high resolution data were on hand were inspected for confirmation of the validity of the type of reasoning applied above. Although not every case gave the same profile as that of Figure 5, each example appeared to contain a staggered whistler foot clarified by reference to the group velocity surface. We hope to collect a number of these for examination and analysis. Corresponding layered effects and resonances should also be sought in the appropriate particle signatures.

In the future, finite temperature and resonance effects need to be added to the analytic sketches. Most importantly, the frequency regime at and below f_{ci}, which is indistinguishable from the $\theta - f$ plane in the plots of U_ϕ and U_g presented here, must be examined for its relationship to the major structural features of the quasi-parallel shock, namely, large and small pulsations with $f/f_{ce} \lesssim 0.001$. We speculate that the whistler mode may play a significant role in the transition from quasi-perpendicular to quasi-parallel structure, inasmuch as wave energy in the mode can penetrate the solar wind upstream in wide ranges of frequency and direction.

Acknowledgments. Material for this report was prepared under National Aeronautics & Space Administration Contracts NASW-3211, NASW-3427, and NASW-3087 (at TRW), NAS5-25772 (at UCLA), and NAS-5-20093 (at University of Iowa).

The Editor thanks B. T. Tsurutani for his assistance in evaluating this paper.

REFERENCES

Al'pert, J., Forty years of whistlers, *J. Atmos. Terr. Phys., 42,* 1, 1980.

Coroniti, F. V., F. L. Scarf, C. F. Kennel, W. S. Kurth, and D. A. Gurnett, Detection of Jovian whistler mode chorus: Implications for the Io torus aurora, *Geophys. Res. Lett., 7,* 45, 1980.

Diodato, L., G. Moreno, C. Signorini, and K. W. Ogilvie, Long-term variations of the solar wind proton parameters, *J. Geophys. Res., 79,* 5095, 1974.

Fairfield, D. H., Whistler waves observed upstream from collisionless shocks, *J. Geophys. Res., 79,* 1368, 1974.

Fairfield, D. H., and W. C. Feldman, Standing waves at low mach number laminar bow shocks, *J. Geophys. Res., 80,* 515, 1975.

Formisano, V., and C. F. Kennel, Small amplitude waves in high β plasmas, *J. Plasma Physics, 3,* 55, 1969.

Formisano, V., G. Moreno, and E. Amata, Relationships among the interplanetary plasma parameters: HEOS 1, December 1968 to December 1969, *J. Geophys. Res., 79,* 5109, 1974.

Greenstadt, E. W., and R. W. Fredricks, Shock systems in collisionless space plasmas, *Solar System Plasma Physics,* vol. 3, edited by C. F. Kennel, L. J. Lanzerotti, and E. N. Parker, p. 4, North-Holland, Amsterdam, 1979.

Greenstadt, E. W., C. T. Russell, F. L. Scarf, V. Formisano, and M. Neugebauer, Structure of the quasi-perpendicular, laminar bow shock, *J. Geophys. Res., 80,* 502, 1975.

Guha, J. K., D. L. Judge, and J. H. Marburger, OGO 5 magnetic-field data near the earth's bow shock: A correlation with theory, *J. Geophys. Res., 77,* 604, 1972.

Gurnett, D. A., F. L. Scarf, R. W. Fredricks, and E. J. Smith, The ISEE 1 and ISEE 2 plasma wave investigation, *IEEE Trans. Geosci. Electron., GE-16,* 225, 1978.

Heppner, J. P., M. Sugiura, T. L. Skillman, B. G. Ledley, and H. M. Campbell, OGO-A magnetic field observations, *J. Geophys. Res., 72,* 5417, 1967.

Menietti, J. D., and D. A. Gurnett, Whistler propagation in the Jovian magnetosphere, *Geophys. Res. Lett., 7,* 49, 1980.

Olson, J. V., R. E. Holzer, and E. J. Smith, High-frequency magnetic fluctuations associated with the earth's bow shock, *J. Geophys. Res., 74,* 4601, 1969.

Perez, J. K., and T. G. Northrop, Stationary waves produced by the earth's bow shock, *J. Geophys. Res., 75,* 6011, 1970.

Rodriguez, P., and D. A. Gurnett, Electrostatic and electromagnetic turbulence associated with the earth's bow shock, *J. Geophys. Res., 80,* 19, 1975.

Rodriguez, P., and D. A. Gurnett, Correlation of bow shock plasma wave turbulence with solar wind parameters, *J. Geophys. Res., 81,* 2871, 1976.

Smith, E. J., R. H. Holzer, M. G. McLeod, and C. T. Russell, Magnetic noise in the magnetosheath in the frequency range 3–300 Hz, *J. Geophys. Res., 72,* 4803, 1967.

Stix, T. H., *The Theory of Plasma Waves,* McGraw-Hill, New York, 1962.

(Received July 31, 1980;
revised October 22, 1980;
accepted October 24, 1980.)